J|A|C|S
ARTICLES
Published on Web 05/17/2007

Self-Organization of *All-Inorganic* Dodecatungstophosphate Nanocrystallites

Keigo Okamoto, Sayaka Uchida, Takeru Ito, and Noritaka Mizuno*

Contribution from the Department of Applied Chemistry, School of Engineering, The University of Tokyo, 7-3-1 Hongo, Bunkyo-ku, Tokyo 113-8656, Japan

Received January 31, 2007; E-mail: tmizuno@mail.ecc.u-tokyo.ac.jp

Abstract: The crystallinity and porosity of *all-inorganic* dodecatungstophosphate $M_3PW_{12}O_{40}$ (M = Cs, NH_4, Ag, denoted as MPW) particles are controlled by the changes in the synthetic temperatures and countercations. The MPW particles can be classified into three groups by the crystallinity and porosity: (i) mesoporous "disordered" aggregates, (ii) microporous "self-organized" aggregates, and (iii) nonporous single crystals. The formation and growth mechanism of MPW particles is expressed by three steps: formation of nanocrystallites, assembly of the nanocrystallites to form aggregates, and the growth of aggregates by the attachment of nanocrystallites. The time courses of the turbidity of the synthetic solution, the concentration of the nanocrystallites, and the average particle sizes of MPW particles are well reproduced by the calculation based on the mechanism.

Introduction

Self-organization is the spontaneous aggregation of molecules or particles into patterns or structures.[1−9] The driving forces of the self-organization are van der Waals interaction, hydrophobic interaction, aromatic interaction, hydrogen-bonding, electrostatic interaction, etc.[1−4] For example, in the synthesis of inorganic metal oxide molecular sieves, the metal oxide framework precursors are formed by the progressive hydrolysis and condensation of metal aquo ions,[10,11] and the organization of the pore structure is achieved by the electrostatic interaction between the precursors and the structure-directing organic molecules.[4,12] In the self-organization of inorganic particles such as metals, metal oxides, and metal sulfides, the control of the shape and size is achieved also by the addition of organic or organometallic molecules, which act as precursors or structure-directing reagents.[2,3,5,6,12−16] For example, the inorganic hydroxyapatite crystallizes along the organic collagen fibers to form the structure of bone tissue, in nature.[6] The morphologies (cubic, dodecahedron, or sphere) of molybdenum oxide particles are controlled by the use of polyethylene oxide homopolymer with different molar masses, which act as a structure-directing reagent.[16] The self-organization of *all-inorganic* aggregates without the aid of organics is reported only for copper sulfate pentahydrate,[17] calcium carbonate,[18] silica carbonate,[19] and tin oxide.[20] While the thermodynamic morphology of the aggregates can be predicted from their crystal structures, most shapes are empirically controlled by changing the extent of supersaturation.[21,22] In addition, the crystallinity and porosity of all-inorganic aggregates have not yet been controlled and the mechanism of the formation and growth is still unclear.

Polyoxometalates are inorganic metal oxide anion nanoclusters that show unique chemical properties such as catalysis by changes in the constituent elements and countercations.[23−31] The dodecatungstophosphoric acid $H_3PW_{12}O_{40}$ is a well-known solid acid, and the partial substitution of protons with alkali metal

(1) Whitesides, G. M.; Grzybowski, B. *Science* **2002**, *295*, 2418.
(2) Cölfen, H.; Mann, S. *Angew. Chem., Int. Ed.* **2003**, *42*, 2350.
(3) Katz, E.; Willner, I. *Angew. Chem., Int. Ed.* **2004**, *43*, 6042.
(4) Barton, T. J.; Bull, L. M.; Klemperer, W. G.; Loy, D. A.; McEnaney, B.; Misono, M.; Monson, P. A.; Pez, G.; Scherer, G. W.; Vartuli, J. C.; Yaghi, O. M. *Chem. Mater.* **1999**, *11*, 2633.
(5) Cha, J. N.; Stucky, G. D.; Morse, D. E.; Deming, T. J. *Nature* **2000**, *403*, 289.
(6) Hartgerink, J. D.; Beniash, E.; Stupp, S. I. *Science* **2001**, *294*, 1684.
(7) Seeman, N. C. *Nature* **2003**, *421*, 427.
(8) Garibotti, A. V.; Knudsen, S. M.; Ellington, A. D.; Seeman, N. C. *Nano Lett.* **2006**, *6*, 1505.
(9) Tanaka, K.; Clever, G. H.; Takezawa, Y.; Yamada, Y.; Kaul, C.; Shionoya, M.; Carell, T. *Nat. Nanotechnol.* **2006**, *1*, 190.
(10) Livage, J. *Stud. Surf. Sci. Catal.* **1994**, *85*, 1.
(11) Livage, J. *Chem. Mater.* **1991**, *3*, 578.
(12) Kirschhock, C. E. A.; Ravishankar, R.; Jacobs, P. A.; Martens, J. A. *J. Phys. Chem. B* **1999**, *103*, 11021, and references therein.
(13) Watzky, M. A.; Finke, R. G. *Chem. Mater.* **1997**, *9*, 3083.
(14) Libert, S.; Gorshkov, V.; Goia, D.; Matijevi, E.; Privman, V. *Langmuir* **2003**, *19*, 10679.
(15) King, S.; Hyunh, K.; Tannenbaum, R. *J. Phys. Chem. B* **2003**, *107*, 12097.
(16) Chen, J.; Burger, C.; Krishnan, C. V.; Chu, B. *J. Am. Chem. Soc.* **2005**, *127*, 14140.
(17) Bright, N. F. H.; Garner, W. E. *J. Chem. Soc.* 1934, 1872.
(18) Davis, K. J.; Dove, P. M.; De Yoreo, J. J. *Science* **2000**, *290*, 1134.
(19) García-Ruiz, J. M.; Hyde, S. T.; Carnerup, A. M.; Christy, A. G.; Van Kranendonk, M. J.; Welham, N. J. *Science* **2003**, *302*, 1194.
(20) Ohgi, H.; Maeda, T.; Hosono, E.; Fujihara, S.; Imai, H. *Cryst. Growth Des.* **2005**, *5*, 1079.
(21) Piana, S.; Reyhani, M.; Gale, J. D. *Nature* **2005**, *438*, 70.
(22) Melia, T. P.; Moffitt, W. P.*J. Colloid Sci.* **1964**, *19*, 433.
(23) Pope, M. T.; Müller, A. *Angew. Chem., Int. Ed.* **1991**, *30*, 34.
(24) Okuhara, T.; Mizuno, N.; Misono, M. *Adv. Catal.* **1996**, *41*, 113.
(25) Hill, C. L., Ed. Polyoxometalates. *Chem. Rev.* **1998**, *98*, 1.
(26) Neumann, R. *Prog. Inorg. Chem.* **1998**, *47*, 317.
(27) Yamase, T., Pope, M. T., Eds. *Polyoxometalate Chemistry for Nano-Composite Design*; Kluwer: Dordrecht, The Netherlands, 2002.
(28) Kozhevnikov, I. V. *Catalysis by Polyoxometalates*; Wiley: Chichester, UK, 2002.
(29) Hill, C. L. In *Comprehensive Coordination Chemistry II*; McClerverty, J. A., Meyer, T. J., Eds.; Elsevier: Amsterdam, 2003; p 679.
(30) Neumann, R. In *Modern Oxidation Methods*; Bäckvall, J. E., Ed.; Wiley-VCH: Weinheim, 2004; p 223.
(31) Mizuno, N.; Kamata, K.; Yamaguchi, K. *Surface and Nanomolecular Catalysis*; Taylor and Francis Group, LLC: New York, 2006; p 463.

10.1021/ja070694c CCC: $37.00

Table 1. Properties of Various MPW Particles[a]

sample	synthetic temperature (K)	solubility (10^{-5} mol dm^{-3})	size of organized form (nm)	ED pattern	major pore	BET surface area (m^2 g^{-1})	*d*(BET) (nm)	*L*(XRD) (nm)	organized form
CsPW	298	0.221	3−10	ring	mesopore	148	6	13	i
	368	1.30	1×10^2 to 3×10^2	spot	micropore	82	12	24	ii
NH_4PW	298	1.22	1×10^2 to 4×10^2	spot	micropore	91	11	27	ii
	368	5.20	3×10^2 to 1×10^3	spot	micropore	51	19	59	ii
	473	250	2×10^4 to 1×10^5	spot	none	9	1.1×10^2	9.3×10^2	iii
AgPW	298	149	5×10^2 to 3×10^3	spot	none	4	2.4×10^2	7.7×10^2	iii
	368	254	2×10^3 to 1×10^4	spot	none	4	2.4×10^2	5.6×10^2	iii

[a] Size of organized form was measured from the SEM image. *d*(BET) (nm) is the average size of nanocrystallites calculated from the BET surface area assuming a spherical shape. *L*(XRD) is the length of coherent ordered structure calculated by Scherrer's equation from the 222 diffraction. Organized forms are (i) mesoporous disordered nanocrystallites, (ii) microporous self-organized aggregates of nanocrystallites, and (iii) nonporous single crystals.

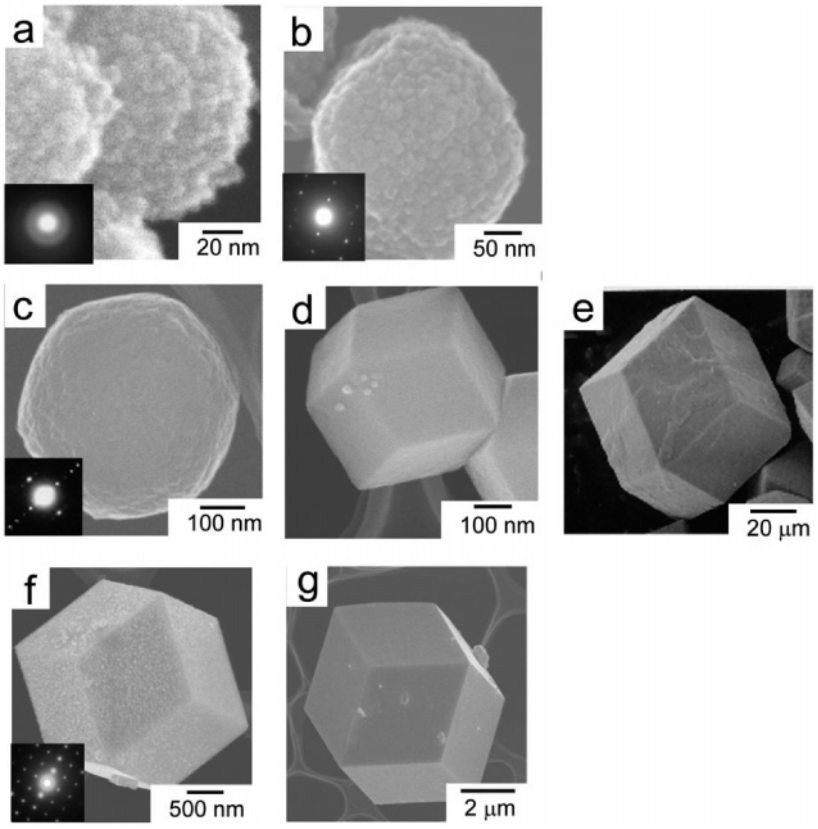

Figure 1. SEM images and ED patterns of (a) CsPW-298, (b) CsPW-368, (c) NH_4PW-298, (d) NH_4PW-368, (e) NH_4PW-473, (f) AgPW-298, and (g) AgPW-368.

ions or ammonium ions increases the surface area and porosity.[4,32−35] For example, $Cs_{2.5}H_{0.5}PW_{12}O_{40}$ possesses high porosity and surface acidity and is more active than the parent acid for acid-catalyzed reaction such as alkylation, acylation, and hydrolysis.[32,34,35] Recently, self-organized aggregates of polyoxometalates have been reported.[36−43] Porous $M_3PW_{12}O_{40}$ (M = NH_4, Cs, denoted as MPW) are self-organized aggregates of 5−10 nm nanocrystallites, while the self-organization is not controllable and the mechanism is still unclear.[4,41−43] On the other hand, ring-shaped polyoxometalate clusters are formed by the self-organization of several tens to more than a hundred molybdenum atoms in acidic solution with reducing reagents[38] or under UV irradiation.[39] These molybdenum oxide clusters further assemble with ionic interactions to form vesicles of ca. 50 nm in size.[40]

In this work, we demonstrate the successful control of the self-organization of *all-inorganic* ionic nanocrystallites by using MPWs and elucidate the self-organization mechanism.

Experimental Section

Materials. $H_3PW_{12}O_{40}\cdot nH_2O$ ($n \approx 25$) was synthesized and purified by extraction with diethyl ether and recrystallization from water.[44] The IR spectrum of $H_3PW_{12}O_{40}\cdot nH_2O$ (KBr: 1079, 982, 892, and 800 cm^{-1})

(32) Nishimura, T.; Okuhara, T.; Misono, M. *Appl. Catal.* **1991**, *73*, L7.
(33) Lapham, D.; Moffat, J. B. *Langmuir* **1991**, *7*, 2273.
(34) Essayem, N.; Coudrier, G.; Fournier, M.; Vedrine, J. C. *Catal. Lett.* **1995**, *34*, 223.
(35) Corma, A.; Martinez, M.; Martinez, C. *J. Catal.* **1996**, *164*, 422.
(36) Long, D. L.; Cronin, L. *Chem.−Eur. J.* **2006**, *12*, 3698.
(37) Rhule, J. T.; Neiwert, W. A.; Hardcastle, K. I.; Do, B. T.; Hill, C. L. *J. Am. Chem. Soc.* **2001**, *123*, 12101.
(38) Müller, A.; Shah, S. Q. N.; Bögge, H.; Schmidtmann, M. *Nature* **1999**, *397*, 48.
(39) Yamase, T.; Prokop, P. V. *Angew. Chem., Int. Ed.* **2002**, *41*, 466.
(40) Liu, T.; Diemann, E.; Li, H.; Dress, A. W. M.; Müller, A. *Nature* **2003**, *426*, 59.
(41) Mizuno, N.; Misono, M. *Chem. Lett.* **1987**, 967.
(42) Ito, T.; Inumaru, K.; Misono, M. *J. Phys. Chem. B* **1997**, *101*, 9958.
(43) Okuhara, T.; Watanabe, H.; Nishimura, T.; Inumaru, K.; Misono, M. *Chem. Mater.* **2000**, *12*, 2230.
(44) Bailar, J. C., Jr. *Inorg. Synth.* **1939**, *1*, 132.

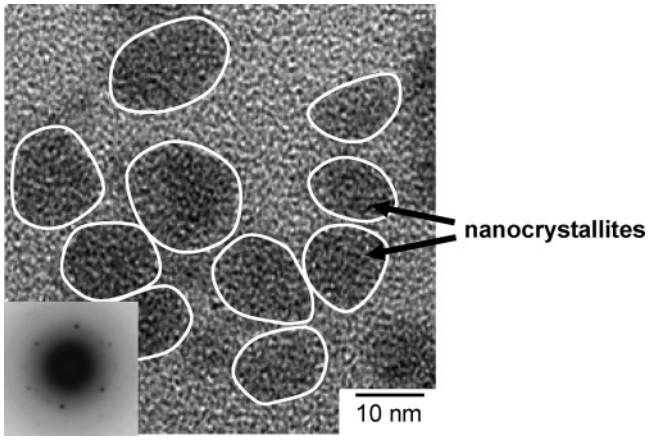

Figure 2. TEM image and ED pattern of CsPW-298 nanocrystallites.

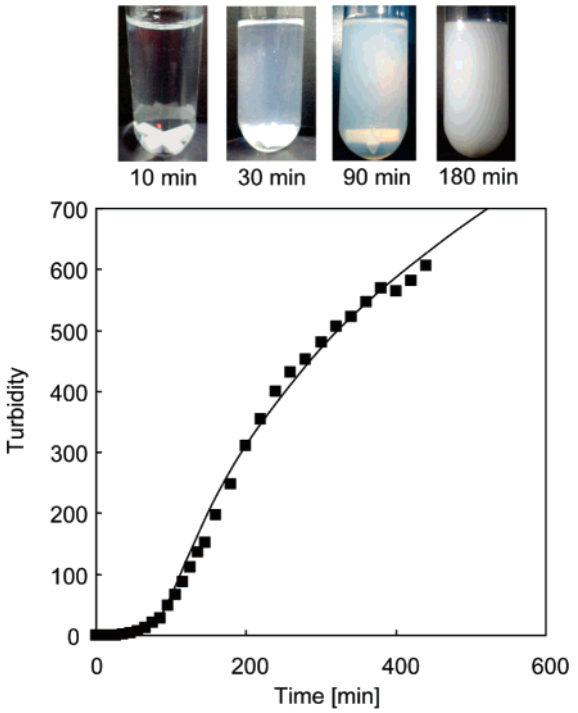

Figure 3. Time courses of the photographs of the synthetic solution of NH_4PW-293 and turbidity. Solid squares and solid line show the experimental and calculated data with eq 3, respectively.

agreed with that reported in the literature.[44] NH_4HCO_3 (Nacalai Tesque) was recrystallized in a water−ethanol mixed solvent. Cs_2CO_3 (Merck) and $AgNO_3$ (Wako) were used without further purification. Water was purified by Milli-RX12α (Millipore Corporation).

Synthesis. MPWs (M = NH_4, Cs, and Ag) were synthesized as follows: A stoichiometric amount of an aqueous solution of NH_4HCO_3, Cs_2CO_3, or $AgNO_3$ (0.075 mol dm^{-3} of M) was added dropwise to an aqueous solution of $H_3PW_{12}O_{40}{\cdot}nH_2O$ (0.025 mol dm^{-3} of $PW_{12}O_{40}^{3-}$) for 5 min with stirring to form a white colloidal solution. During this procedure, the solution was kept at 298 or 368 K. NH_4PW-473 was synthesized under hydrothermal conditions as described before.[45] For the mechanistic study, the synthetic solution of NH_4PW was prepared by adding an aqueous solution (15 mL) of $H_3PW_{12}O_{40}{\cdot}nH_2O$ (0.005 mol dm^{-3}) to an aqueous solution (15 mL) of NH_4HCO_3 (0.015 mol dm^{-3}) in a single step with stirring at 293 K. The synthetic solution of CsPW was prepared by adding an aqueous solution (15 mL) of $H_3PW_{12}O_{40}{\cdot}nH_2O$ (0.001 mol dm^{-3}) to an aqueous solution (15 mL) of Cs_2CO_3 (0.0015 mol dm^{-3}) in a single step with stirring at 293 K.

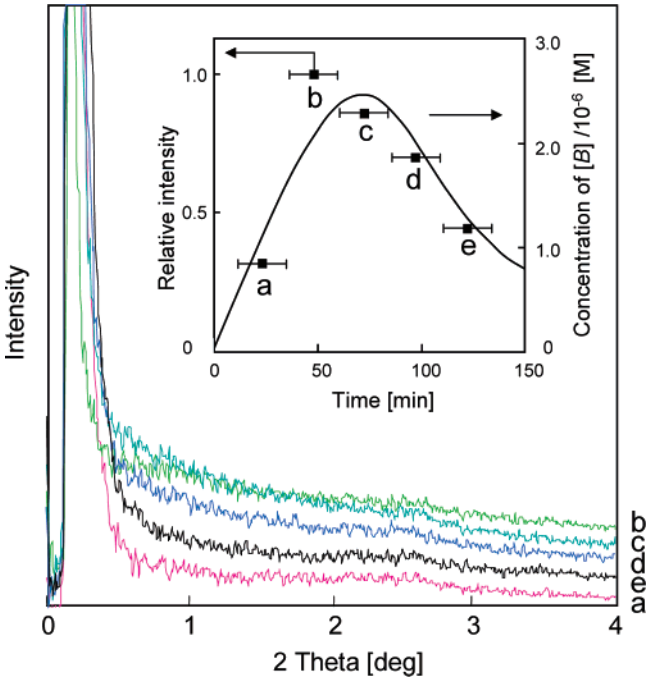

Figure 4. Time course of the SAXS profiles of the synthetic solution of NH_4PW-293. Inset: the relative signal intensity at $2\theta = 2.52°$ in the SAXS profile. The solid line shows the concentration of [*B*] calculated with eq 9. The SAXS profiles were the averaged data for (a) 13−33 min, (b) 38−58 min, (c) 62−82 min, (d) 87−107 min, and (e) 112−132 min.

Characterization. The scanning electron microscopy (SEM) images were obtained with an S-4700 (Hitachi) without metal coating. The transmission electron microscopy (TEM) images and electron diffraction (ED) patterns were measured with a JEM-4000FX II (JEOL). The TEM image and ED pattern of Cs-298 were measured with a JEM-2100 (JEOL) at 77 K: CsPW-298 was dispersed in a resin and the resin was sliced with a microtome to a thickness of 50 nm. N_2 adsorption/desorption isotherms of MPW were measured with an ASAP-2010 automatic adsorption apparatus (Micromeritics). Powder X-ray diffraction patterns were recorded with a MultiFlex diffractometer (Rigaku Corporation) using Cu Kα radiation.

The solubility of MPW was estimated as follows: MPW was dispersed in water at 298 or 368 K, and the quantity of $PW_{12}O_{40}^{3-}$ in the supernatant was estimated with the absorbance of the 260 nm band of the Keggin anion (ligand-to-metal charge transfer (O→W) band). The solubility in water at 368 K was also estimated by using the surface free energy ($\bar{\gamma}$) at 298 K. The value of $\bar{\gamma}$ was calculated with the equation $r_{cn} = 2\bar{\gamma}V/(kT\ln(a/a_0))$, where r_{cn}, k, T, and V are the size of the critical nuclei, Boltzmann constant (1.38066×10^{-23} J K^{-1}), temperature, and molecular volume (4.189×10^{-27} m^3), respectively.[46] Concentrations were used in place of approximated activities (a_0, initial concentration of $H_3PW_{12}O_{40}$ (0.025 mol dm^{-3}); a, solubility of MPW). The estimated values of the solubility approximately agreed with the experimental values (e.g., experimental (estimated) solubility of Cs-368: 17.5 (13.0) μmol dm^{-3}).

Small-angle X-ray scattering (SAXS) measurements of the synthetic solution were carried out to detect nanocrystallites with a NANO-Viewer diffractometer (Rigaku Corporation). The solution was sealed in a quartz capillary (2 mm ϕ), and the SAXS spectra were measured with Cu Kα radiation (40 kV, 20 mA).

(45) Ito, T.; Hashimoto, M.; Uchida, S.; Mizuno, N. *Chem. Lett.* **2001**, 1272.

(46) Stumm, W. *Chemistry of the Solid-Water Interface*; Wiley: New York, 1992.

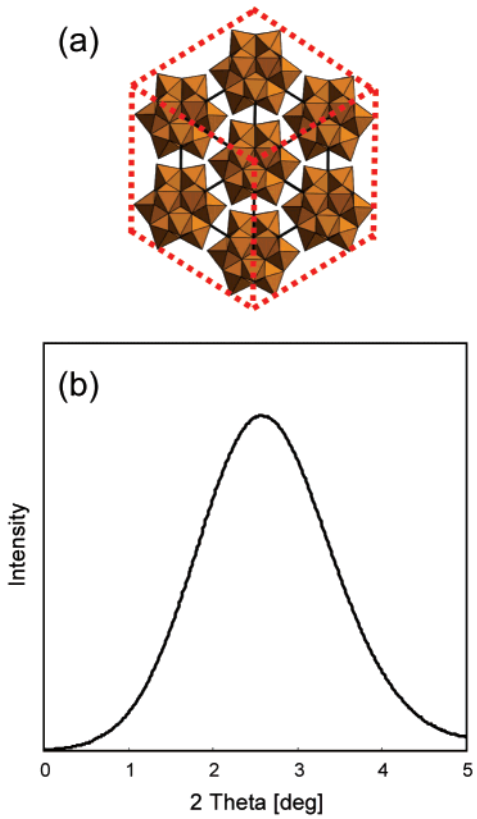

Figure 5. (a) Schematic model of a nanocrystallite of ca. 3 nm in size and (b) the calculated X-ray diffraction pattern. Gray polyhedron shows the WO_6 unit of $PW_{12}O_{40}^{3-}$.

UV−vis spectra of the synthetic solution were measured in the range 200−800 nm with a Fiberspec S-2450 (Soma). The absorbance (A) was converted to the turbidity (τ) with the equation $\tau = 2.303A$. The turbidity (τ) of the solution is defined by

$$\frac{I}{I_0} = \exp(-\tau l) \tag{1}$$

where I/I_0 and l are the transmittance of light and the length of the light pass, respectively.[47] According to Rayleigh−Gans theory[48,49] the turbidity of the solution containing spherical particles is defined by

$$\frac{\tau}{c} = \frac{4\pi\alpha^3}{\lambda d}\left(\frac{m^2-1}{m^2+2}\right)^2 \tag{2}$$

where c, d, λ, a, and m are the concentration of the particle [g cm^{-3}], density of the particle, wave length in water, relative particle size, and relative refractive index, respectively. The density of the particle, relative particle size, and relative refractive index are defined by $d = M/V_pN_A$ (M, molecular weight; V_p, volume of particle ($=4/3\pi r^3$); N_A, Avogadro's number), $\alpha = 2\pi r/\lambda$, and $m = \mu_1/m_2$ (μ_1, refractive index of water (1.33); μ_2, refractive index of particle (1.68)),[50] respectively.

(47) Atkins, P. W. *Physical Chemistry*; Oxford University Press: Oxford, 1990; Chapter 17.
(48) Lord Rayleigh. *Proc. R. Soc.* **1911**, *A84*, 25.
(49) Gans, R. *Ann. Phys.* **1925**, *76*, 29.
(50) The best fit for the calculation of the turbidity of the NH_4PW solution was obtained with $\mu_2 = 1.68$. The value agreed fairly well with the refractive index of typical metal oxides (μ = ca. 1.5) (*American Institute of Physics Handbook*, 3rd ed.; McGrawHill: New York, 1973).

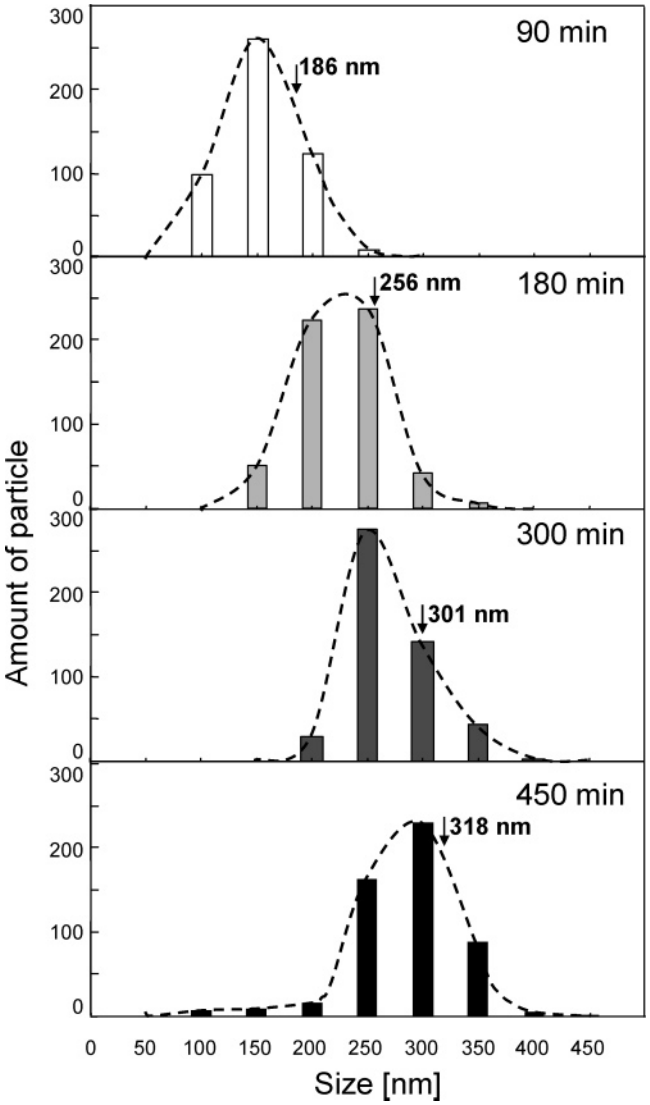

Figure 6. Time course of the particle size distribution of NH_4PW-293. The average particle size is shown by the arrow. Each graph shows the size distribution of 450−550 particles in the SEM images.

In order to apply eq 2 to a wide range of particle sizes, $f(\alpha)$was multiplied by eq 2 for the correction.[51] Equation 3 was obtained by the substitution of the parameters in eq 2:

$$\tau = 1.54 \times 10^{53} \times V_p^2[C] \times f(\alpha) \tag{3}$$

where $[C]$ is particle concentration. The values of $f(\alpha)$ were obtained from ref 51 and were approximated as a linear equation of α,

$$f(\alpha) = \begin{Bmatrix} -0.42\alpha + 1.12\ (0 < \alpha < 2) \\ -0.172\alpha + 0.63\ (2 \le \alpha < 2.5) \\ -0.069\alpha + 0.36\ (2.5 \le \alpha < 4) \\ -0.030\alpha + 0.21\ (4 \le \alpha < 5) \\ -0.012\alpha + 0.12\ (5 \le \alpha < 6) \end{Bmatrix} \tag{4}$$

(51) Tabibian, R. M.; Heller, W.; Epel, J. N. *J. Colloid Sci.* **1956**, *11*, 195: Theoretical turbidity calculated by eq 2 is compared to the experimental one for polymer solution, of which the concentration and particle size are known. The deviation between the theretical and experimental values are corrected by the multiplication of $f(\alpha)$.

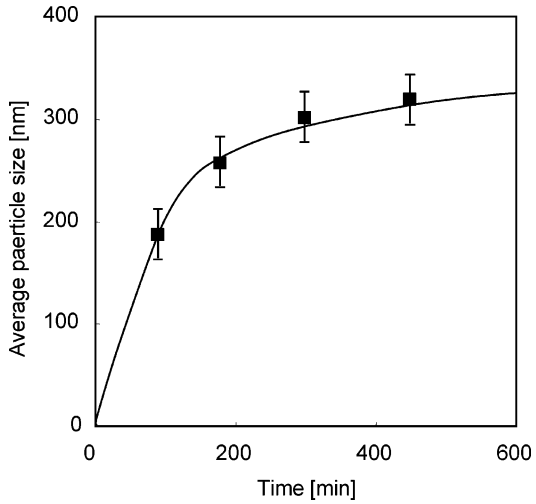

Figure 7. Time course of the average particle size of NH_4PW-293. Solid squares and solid line show the experimental and calculated data with eq 14, respectively.

Results and Discussion

Systematic Control of Crystallinity and Porosity of MPW Particles with Temperature and Countercations. Table 1 and Figure 1 show the properties and SEM images of MPW particles, respectively. The morphology (SEM) and crystallinity (ED) of the MPW particles systematically changed with changes in the synthetic temperatures and the kinds of countercations as follows: CsPW synthesized at 298 K (designated as CsPW-298) consisted of fine nanocrystallites of <10 nm in size (Figure 1a). The nanocrystallites formed spherical aggregates of 50−100 nm in size and were crystallographically disordered, as indicated by the ring-patterned electron diffractogram (ED). The ED of the nanocrystallites showed discrete spots, indicating that the nanocrystallites are crystalline (Figure 2). The intercrystallite spaces behaved as mesopores.[41,43] By increasing the synthetic temperature to 368 K (CsPW-368), the sizes of spherical particles were increased to 100−300 nm (Figure 1b). The particles showed discrete spots in the ED, indicating that the nanocrystallites are crystallographically ordered in the spherical particles (i.e., self-organized aggregates).

By changing the countercation from Cs^+ to NH_4^+, spherical particles of 100−400 nm in size were formed at 298 K (NH_4-PW-298) (Figure 1c). The large BET surface area (91 $m^2\ g^{-1}$) indicates that the spherical particles are aggregates of nanocrystallites of ca. 10 nm in size. The ED of NH_4PW-298 showed discrete spots, indicating that the nanocrystallites are crystallographically ordered in the same way as that of CsPW-368.

By increasing the synthetic temperature to 368 K, dodecahedral particles were formed and the sizes were increased to 0.3−1 μm (Figure 1d). The dodecahedron was formed by 12 equivalent planes of {110} of a cubic lattice. Generally, the morphology of self-organized aggregates of a material with a cubic lattice is either a cube[52] formed by six equivalent planes of {100} or a dodecahedron[53] formed by 12 equivalent planes of {110}. In the case of NH_4PW, the single crystal grown under hydrothermal conditions showed a cubic cell (space group, $Pn3\text{-}m$),[45] and the powder XRD patterns of the other MPWs were indexed to the same structure. In the unit cell, polyoxometalates were placed at the vertices of the cube and were positioned diagonally. Therefore, the density of the {110} planes was higher than that of {100}, suggesting that the crystal growth along the {110} planes to form a dodecahedron is thermodynamically more stable than that along the {100} planes to form a cube. The BET surface area of NH_4-PW-368 was 51 $m^2\ g^{-1}$ and still had a large micropore volume. Nonporous dodecahedral single crystals of 25 μm in size were grown under hydrothermal conditions (NH_4PW-473, Figure 1e).[45]

By changing the countercation to Ag^+, nonporous dodecahedral particles of 0.5−3 μm in size were formed even at 298 K (AgPW-298) (Figure 1f). By increasing the synthetic temperature to 368 K (AgPW-368), the particle size was increased to 2−10 μm (Figure 1g). Thus, MPW particles can be classified into three groups by their crystallinity and porosity: (i) mesoporous "disordered" aggregates (CsPW-298), (ii) microporous "self-organized" aggregates (CsPW-368, NH_4PW-

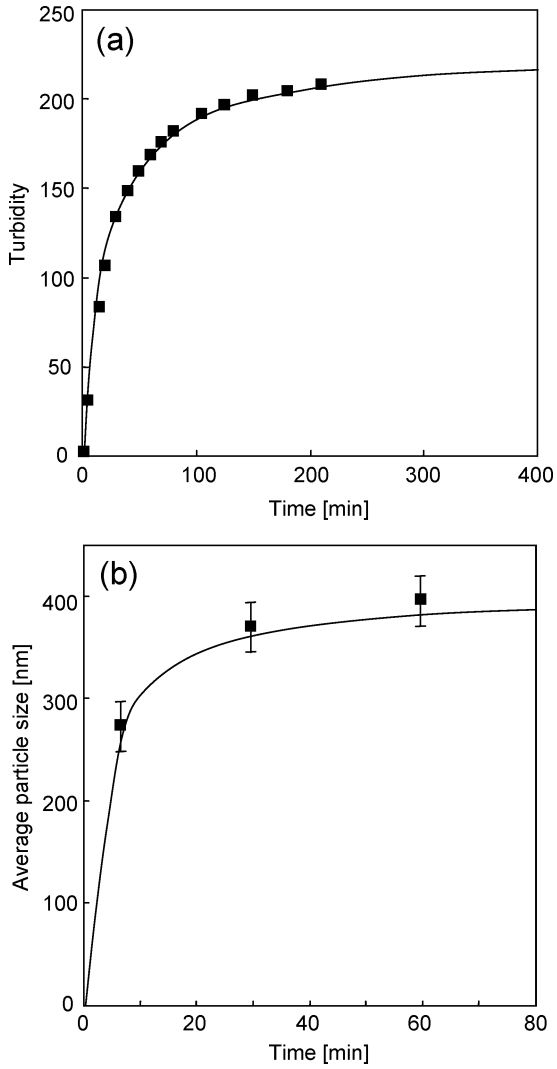

Figure 8. Time courses of the (a) turbidity of the synthetic solution and (b) averag particle size of CsPW-293. Solid squares and solid lines show the experimental and calculated data, respectively.

(52) Lu, W.; Fang, J.; Stokes, K. L.; Lin, J. *J. Am. Chem. Soc.* **2004**, *124*, 11798.
(53) Trikalitis, P. N.; Rangan, K. K.; Bakas, T.; Kanatzidis, M. G. *J. Am. Chem. Soc.* **2002**, *126*, 12255.

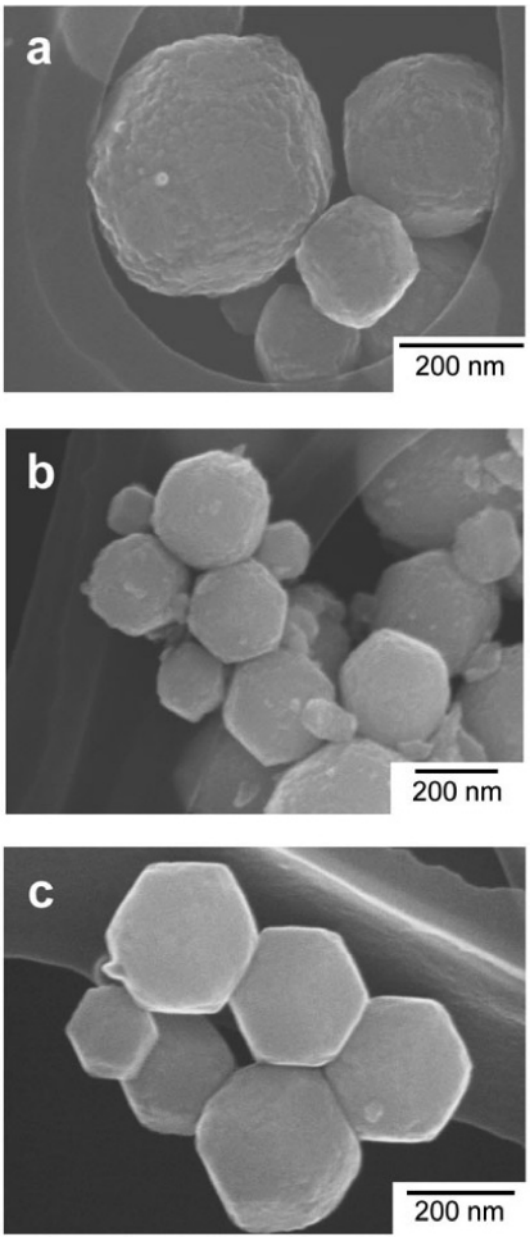

Figure 9. SEM images of NH_4PW-298 particles: (a) as prepared and after keeping in water (b) at 298 K for 1 week and (c) at 368 K for 24 h.

298, and NH_4PW-368), and (iii) nonporous single crystals (NH_4PW-473, AgPW-298, and AgPW-368).[54]

Formation and Growth of NH_4PW Particles.[56] The turbidity of the synthetic solution of NH_4PW-293 can be used as a measure of the aggregation since NH_4PW-293 are white particles of 100−400 nm in size and scatter visible light. Figure 3 shows the photographs of the synthetic solution of NH_4PW-293 and the turbidity. The solution was initially clear and then became cloudy with time. The turbidity showed an induction period and then increased with time, in good agreement with the photographs.

Figure 4 shows the reproducible changes in the SAXS profiles of the synthetic solution as a function of time. The intensity of the $2\theta = 2-3°$ region ($d = 3-4.5$ nm) initially increased, reached a maximum around 50 min, and then decreased. This peak position approximately agreed with that calculated with dodecahedral NH_4PW-293 nanocrystallites of 3 nm in size (Figure 5). Therefore, the initial increase in the intensity of the $2\theta = 2-3°$ region suggests that the nanocrystallites are initially formed and then the amount decreased with time.

The increase in the turbidity after the induction period in Figure 3 and the decrease in the signal intensity of $2\theta = 2-3°$ suggest that the formation and growth of particles take place by the consumption of the nanocrystallites. Figure 6 shows the time course of the particle size distribution of NH_4PW-293. The size increased, while the distribution remained almost unchanged with time, showing that the particles are monodispersed.

Kinetics and Mechanism. On the basis of the above results, it is probable that the formation and aggregation of nanocrystallites proceeds according to eqs 5−7; nanocrystallites are formed with free $PW_{12}O_{40}^{3-}$ and M^+ (eq 5) and assemble to form aggregates (eq 6), and then the aggregates grow by attaching nanocrystallites (eq 7) (Scheme S1).

$$A \xrightarrow{k_1} B \text{ (nucleation)} \tag{5}$$

$$B + B \xrightarrow{k_2} C \text{ (formation)} \tag{6}$$

$$B + C \xrightarrow{k_3} C \text{ (growth)} \tag{7}$$

where A, B, and C stand for the free ions (NH_4^+, $PW_{12}O_{40}^{3-}$), nanocrystallites, and aggregates, respectively. According to eqs 5−7, the following rate equations were obtained:

$$\frac{d[A]}{dt} = -k_1[A]^2 \tag{8}$$

$$\frac{d[B]}{dt} = \frac{k_1}{n_B}[A]^2 - 2k_2[B]^2 - k_3[B][C] \tag{9}$$

$$\frac{d[C]}{dt} = k_2[B]^2 \tag{10}$$

where k_1 and k_2 are rate constants, k_3 is time dependent,[57] and n_B is the average number of $[PW_{12}O_{40}]^{3-}$ in the nanocrystallite. $[A]$, $[B]$, and $[C]$ could be calculated by solving eqs 8−10 consecutively with $\Delta t = 0.02$ s, and the time courses of the turbidity of the synthetic solution of NH_4PW-293 (Figure 3), the concentration of the nanocrystallites (inset in Figure 4), and the average particle size of NH_4PW-293 (Figure 7) were well reproduced by $k_1 = 1.2$ [s^{-1} mol^{-1} dm^3], $k_2 = 2.5 \times 10^{-1}$ [s^{-1} mol^{-1} dm^3], and $k_3' = 9.9 \times 10^6$ [s^{-1} mol^{-1} dm^3] (see the solid lines). The results suggest that the formation and aggregation of the nanocrystallite is much slower than the growth of the particle (k_1, $k_2 \ll k_3$). All these results support eqs 5−7. The increase in the turbidity after the induction period (Figure 3) and decrease in the signal intensity of $2\theta = 2-3°$ in the SAXS profile (Figure 4) show that the particle growth by the

(54) While MPW particles of groups ii and iii have an epitaxial connection of nanocrystallites and the formation and growth of these particles would be regarded as the crystal growth,[55] the nanocrystallites are randomly oriented (disordered) in the MPW particles of group i. Therefore, the formation and growth of MPW particles in part includes the crystal growth.

(55) Markov, I. *Crystal Growth for Beginners*; World Scientific: Hackensack, NJ, 2003.

(56) The formation and growth of the aggregates was made slower by lowering the concentration of the ions in the synthetic solution of NH_4PW to investigate the mechanism in more detail.

attachment of the nanocrystallites (eq 7) becomes dominant after a certain period (ca. 50 min).

The time courses of the turbidity (Figure 8a) and average particle size (Figure 8b) of CsPW-293 were also well reproduced by the calculation with $k_1 = 2.5 \times 10^2$ [s^{-1} mol^{-1} dm^3], $k_2 = 6.5$ [s^{-1} mol^{-1} dm^3], and $k_3' = 8.1 \times 10^8$ [s^{-1} mol^{-1} dm^3].[62] Thus the mechanism could also be applied to the formation of CsPW particles.

On the basis of the mechanism described above and the reverse reactions (solubilization), the decreases in the crystallinity (crystallographic coherence) and the increases in the porosity (BET surface area) of MPWs with the decrease in the solubility (Table 1) were explained.[63] CsPW-298, with the lowest solubility (group i), did not aggregate into the crystalline form, and the mesopores were left between the nanocrystallites probably because the dissolution and reprecipitation of the nanocrystallites hardly occur. As for the compounds in group ii with medium solubility, the epitaxial interfaces were formed to give a thermodynamically stable morphology (i.e., dodecahedron), and certain amounts of micropores were left between the nanocrystallites. As shown in Figure 9, by keeping NH_4-PW-298 in water (at 298 K for 1 week or at 368 K for 24 h), the morphology of the particle changed from sphere to dodecahedron with a fair maintenance of the particle size. Therefore, epitaxial interfaces are formed by the slight dissolution and reprecipitation of the nanocrystallites. As for the compounds with high solubility (group iii), nonporous dodecahedral crystals were formed probably because the dissolution and reprecipitation of the nanocrystallites easily occur.

Conclusion

The self-organization of all-inorganic nanocrystallites was successfully controlled by the changes in the synthetic temperatures and countercations. The formation and growth mechanism of MPW particles was elucidated by the mechanism that consisted of three steps: formation of nanocrystallites, assembly of the nanocrystallites to form aggregates, and the growth of aggregates by the attachment of nanocrystallites.

Acknowledgment. Mr. Tsunakawa (Univ. of Tokyo) is acknowledged for the measurements of ED patterns. Mr. Endo (JEOL) is acknowledged for the measurements of TEM and ED patterns of Cs-298. Mr. Hoshino (Rigaku Corporation) is acknowledged for the measurements of SAXS patterns. This work was supported in part by the Core Research for Evolutional Science and Technology (CREST) program of the Japan Science and Technology Agency (JST) and a Grant-in-Aid from the Ministry of Education, Culture, Sports, Science, and Technology of Japan.

Supporting Information Available: Scheme S1 shows a schematic illustration of the formation and aggregation of nanocrystallites according to eqs 5−7. This material is available free of charge via the Internet at http://pubs.acs.org.

JA070694C

(57) On the assumption that the growth of the aggregates by attaching nanocrystallites is a diffusion-controlled reaction, the rate of the consumption of nanocrystallites by the attachment to an aggregate is expressed by $k_3 = 4\pi(r + r_{nano})DN_A$ (11), where r, r_{nano}, N_A, and D are the average radius of aggregates, average radius of nanocrystallites ($r_{nano} = 3$ nm), Avogadro's number, and the diffusion constant, respectively.[58] According to the Stokes−Einstein equation, the diffusion constant D is expressed by $D = kT/6\pi\eta(1/r + 1/r_{nano})$ (12), where η is the viscosity of water.[59] The average number of nanocrystallites (n_C) in a monodispersed particle is given by $n_C = (\int_0^t k_3[B][C]\,dt)/[C]$ (13), where V is the volume of the synthetic solution. Thus, the average radius of the aggregate is expressed by[60] $r = r_{nano}n_C^{1/3} \times 1.2$ (14). By the use of eq 14, eq 15 is derived from eq 11 as follows: $k_3 = k_3'(r + r_{nano})(1/r + 1/r_{nano})$ (15), where k_3' is $(2kTN_AA)/3\eta$ and A is a coefficient taking the reverse reaction of eq 7 (dissolution of the aggregate) into account.

(58) Atkins, P. W. *Physical Chemistry*; Oxford University Press: Oxford, 1990; Chapter 28.

(59) Atkins, P. W. *Physical Chemistry*; Oxford University Press: Oxford, 1990; Chapter 25.

(60) The constant 1.2 in eq 14 was calculated with $(0.58)^{-1/3}$, where 0.58 is the typical filling factor of the random packing of spheres.[61]

(61) Privman, V.; Goia, D. V.; Park, J.; Matijevi, E. *J. Colloid Sci.* **1999**, *213*, 36.

(62) The fitting of the turbidity gave $k_3' = 9.9 \times 10^6$ [s^{-1} mol^{-1} dm^3] for NH_4-PW, and the value was smaller than 1.9×10^9 [s^{-1} mol^{-1} dm^3], which was calculated by $k_3' = 2kTN_A/3\eta$ on the assumption that the reverse reaction of eq 7 is negligible (i.e., $A = 1$). The discrepancy was probably due to the contribution of the dissolution of the aggregates (i.e., reverse reaction of eq 7). On the other hand, the k_3 value (8.1×10^8) for CsPW agreed fairly well with the calculated value (1.9×10^9).

(63) The solubility of MPW in water increases with the increase in the hydration enthalpy of the countercation (Huheey, J. E. *Inorganic Chemistry*; Harper & Row Publishers: New York, 1983; Chapter 3). The hydration enthalpy is proportional to the square of the charge and the inverse of the ionic radius. Therefore, the solubility of MPWs would decrease in the order AgPW (Ag^+, 1.29 Å) > NH_4PW (NH_4^+, 1.51 Å) > CsPW (Cs^+, 1.81 Å), which agreed with the experimental results.